Acta Cryst E CRYSTALLOGRAPHIC COMMUNICATIONS

ISSN 2056-9890

Crystal structure determination, Hirshfeld surface, crystal void, intermolecular interaction energy analyses, as well as DFT and energy framework calculations of 2-(4-oxo-4,5-dihydro-1*H*-pyrazolo-[3,4-*d*]pyrimidin-1-yl)acetic acid

Received 14 July 2022
Accepted 23 August 2022

Edited by M. Weil, Vienna University of Technology, Austria

Keywords: crystal structure; hydrogen bond; C—H···π(ring) interaction; pyrazolopyrimidine.

CCDC reference: 2203303

Supporting information: this article has supporting information at journals.iucr.org/e

Ezaddine Irrou,[a]* Younesse Ait Elmachkouri,[a] Ali Oubella,[a,b] Hassan Ouchtak,[a] Samira Dalbouha,[c,d] Joel T. Mague,[e] Tuncer Hökelek,[f] Lhoussaine El Ghayati,[g] Nada Kheira Sebbar[a,g] and Mohamed Labd Taha[a]

[a]Laboratory of Organic and Physical Chemistry, Applied Bioorganic Chemistry Team, Faculty of Sciences, Ibn Zohr University, Agadir, Morocco, [b]Laboratory of Organic Synthesis and Molecular Physico-Chemistry, Department of Chemistry, Faculty of Sciences, Semlalia, BP 2390, Marrakech 40001, Morocco, [c]Laboratory of Organic Chemistry and Physical Chemistry, Research Team: Molecular Modeling, Materials and Environment, Department of Chemistry, Faculty of Sciences of Agadir, University Ibn Zohr, BP 8106 Agadir, Morocco, [d]Laboratory of Spectroscopy, Molecular Modeling, Materials, Nanomaterials, Water and Environment, CERNE2D, Faculty of Sciences, Mohammed V University in Rabat, Av. Ibn Battouta, BP 1014, Rabat, Morocco, [e]Department of Chemistry, Tulane University, New Orleans, LA 70118, USA, [f]Department of Physics, Hacettepe University, 06800 Beytepe, Ankara, Turkey, and [g]Laboratory of Heterocyclic Organic Chemistry, Medicines Science Research Center, Pharmacochemistry Competence Center, Mohammed V University in Rabat, Faculty of Sciences, Av. Ibn Battouta, BP 1014, Rabat, Morocco. *Correspondence e-mail: ezaddine1996@gmail.com

In the title molecule, $C_7H_6N_4O_3$, the bicyclic ring system is planar with the carboxymethyl group inclined by 81.05 (5)° to this plane. In the crystal, corrugated layers parallel to (010) are generated by N—H···O, O—H···N and C—H···O hydrogen-bonding interactions. The layers are associated through C—H···π(ring) interactions. A Hirshfeld surface analysis indicates that the most important contributions to the crystal packing are from H···O/O···H (34.8%), H···N/N···H (19.3%) and H···H (18.1%) interactions. The volume of the crystal voids and the percentage of free space were calculated to be 176.30 Å^3 and 10.94%, showing that there is no large cavity in the crystal packing. Computational methods revealed O—H···N, N—H···O and C—H···O hydrogen-bonding energies of 76.3, 55.2, 32.8 and 19.1 kJ mol^{-1}, respectively. Evaluations of the electrostatic, dispersion and total energy frameworks indicate that the stabilization is dominated *via* dispersion energy contributions. Moreover, the optimized molecular structure, using density functional theory (DFT) at the B3LYP/6–311G(d,p) level, was compared with the experimentally determined one. The HOMO–LUMO energy gap was determined and the molecular electrostatic potential (MEP) surface was calculated at the B3LYP/6–31G level to predict sites for electrophilic and nucleophilic attacks.

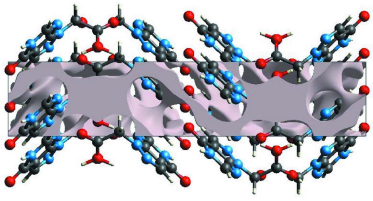

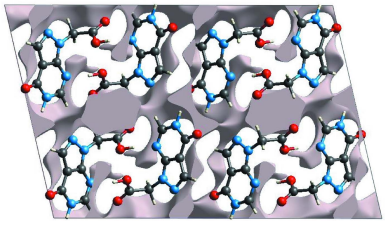

1. Chemical context

The chemistry of heterocyclic compounds still receives increasing interest because of the therapeutic importance of most heterocyclic compounds, especially those with nitrogen-containing heterocycles, which are of great interest as potential bioactive molecules (Taia *et al.*, 2020; Sebbar *et al.*, 2016; El Ghayati *et al.*, 2021; Dinakaran *et al.*, 2012; Lahmidi *et al.*, 2018; Hni *et al.*, 2019). In this regard, pyrazolo[3,4-*d*]pyrimi-]pyrimidines are an important family of heterocyclic compounds, and their derivatives possess various pharmacological properties (Bakavoli *et al.*, 2010; Severina *et al.*, 2016),

including their applications as anti-microbial (Holla *et al.*, 2006; Bakavoli *et al.*, 2010), anti-tumor (Kandeel *et al.*, 2012), anti-inflammatory (El-Tombary, 2013), anti-oxidant (El-Mekabaty, 2015), anti-cancer (Gupta *et al.*, 2008; Maher *et al.*, 2019) and anti-convulsant (Severina *et al.*, 2016) agents. Pyrazolopyrimidines can also be used in the treatment of Alzheimers' disease (Zhang *et al.*, 2018), and they have a powerful activity against herpes viruses (Gudmundsson *et al.*, 2009) and human leukaemia (HL-60) (Song *et al.*, 2011).

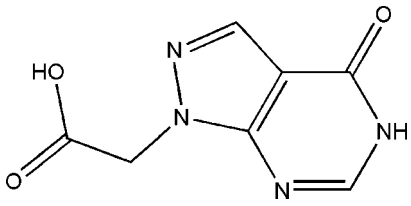

As a continuation of our research in this context, the title compound, (I), was synthesized by basic hydrolysis of the methyl ester of 2-(4-oxo-4, 5-dihydro-1*H*-pyrazolo[3,4-*d*]pyrimidin-1-yl)acetate. We report herein its synthesis, molecular and crystal structures along with Hirshfeld surface analysis, crystal void and intermolecular interaction energies. Moreover, the optimized molecular structure carried out at the B3LYP/6–311 G(d,p) level is compared with the experimentally determined structure, and energy framework as well as molecular electrostatic potential (MEP) surface computations carried out at the B3LYP/6-31G level to predict the reactive sites for the electrophilic and nucleophilic attacks on (I) are presented.

2. Structural commentary

The pyrazolopyrimidine moiety is planar to within 0.0143 (10) Å (r.m.s deviation = 0.0082 Å) with the flap atom N1, which is part of the NH group, being the furthest from the mean plane. The plane of the carboxyl group is inclined to the above plane by 81.05 (5)°. There are no unusual bond lengths or interatomic angles in the molecule (Fig. 1).

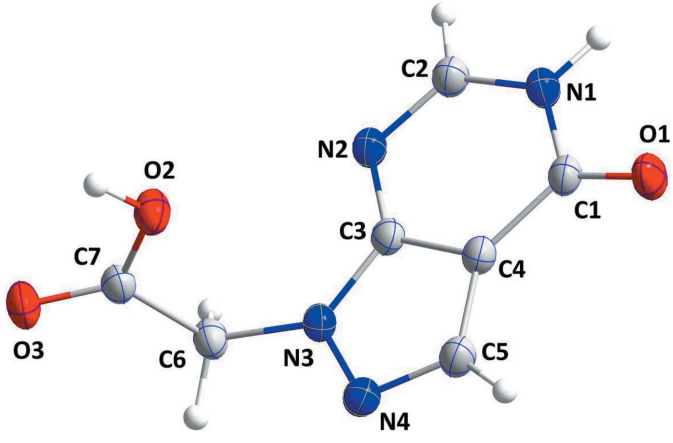

Figure 1
The title molecule with displacement ellipsoids at the 30% probability level.

Table 1
Hydrogen-bond geometry (Å, °).

*Cg*1 is the centroid of the C3/C4/C5/N4/N3 ring.

D—H···*A*	*D*—H	H···*A*	*D*···*A*	*D*—H···*A*
N1—H1···O1^{i}	0.91	1.90	2.8094 (16)	175
O2—H2*A*···N2^{ii}	0.87	1.85	2.7120 (14)	173
C5—H5···O1^{iii}	0.93	2.33	3.2305 (18)	164
C6—H6*A*···O3^{iv}	0.97	2.36	3.2436 (18)	152
C6—H6*B*···*Cg*1^{v}	0.97	2.98	3.7387 (15)	136

Symmetry codes: (i) $-x+1, -y+1, -z+1$; (ii) $-x+\frac{1}{2}, y+\frac{1}{2}, -z+\frac{1}{2}$; (iii) $-x+\frac{1}{2}, -y+\frac{3}{2}, -z+1$; (iv) $-x, y, -z+\frac{1}{2}$; (v) $x, y-1, z$.

3. Supramolecular features

In the crystal, inversion dimers are formed by N1—H1···O1 hydrogen bonds (Table 1) and are connected into sheets by complementary C5—H5···O1 hydrogen bonds (Table 1). Adjacent sheets are connected by O2—H2*A*···N2 and C6—C6*A*···O3 hydrogen bonds (Table 1) to form corrugated (010)

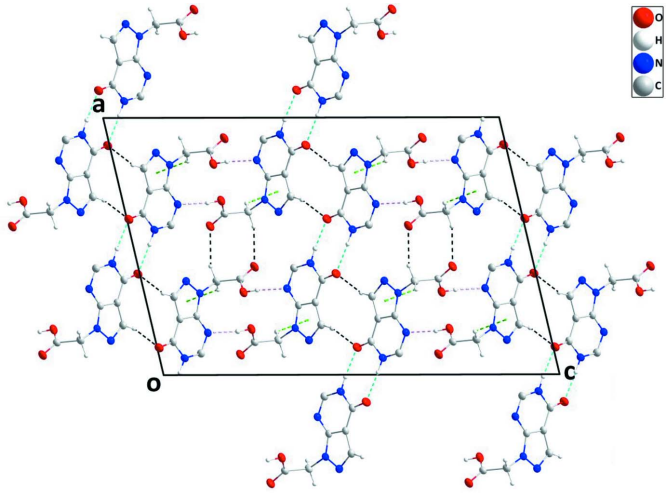

Figure 2
View of the crystal packing along the *b*-axis direction with N—H···O, O—H···N and C—H···O hydrogen bonds shown, respectively, by light-blue, pink and black dashed lines. C—H···π(ring) interactions are shown by green dashed lines.

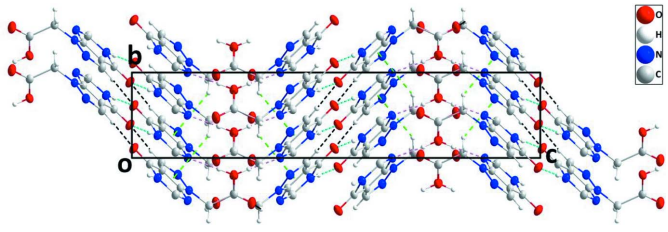

Figure 3
View of the crystal packing along the *a*-axis direction with N—H···O, O—H···N and C—H···O hydrogen bonds shown, respectively, by light-blue, pink and black dashed lines. C—H···π(ring) interactions are shown by green dashed lines.

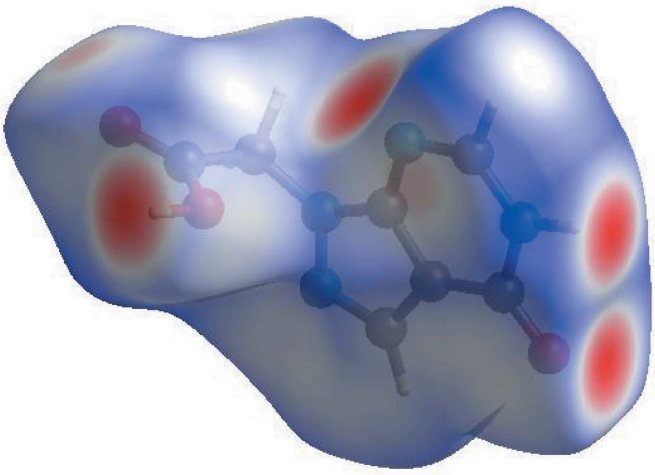

Figure 4
View of the three-dimensional Hirshfeld surface of the title compound, plotted over d_{norm} in the range −0.6986 to 1.3450 a.u.

layers with the component sheets alternately arranged parallel to $(11\bar{6})$ and $(\bar{1}16)$ (Figs. 2 and 3). These corrugated layers are associated through C6—H6*B*···*Cg*1 interactions (Table 1 and Fig. 3).

4. Hirshfeld surface and crystal void analysis

In order to visualize the intermolecular interactions in the crystal of (I), a Hirshfeld surface (HS) analysis (Hirshfeld, 1977) was carried out by using *Crystal Explorer* (Spackman *et al.*, 2021). In the HS plotted over d_{norm} (Fig. 4), the white surface indicates contacts with distances equal to the sum of van der Waals radii, and the red and blue colours indicate distances shorter or longer than the sum of the van der Waals radii, respectively (Venkatesan *et al.*, 2016). The bright-red spots indicate sites of donor and/or acceptor interactions and they also appear as blue and red regions corresponding to positive (hydrogen bond donors) and negative (hydrogen bond acceptors) potentials on the HS mapped over electrostatic potential (Spackman *et al.*, 2008; Jayatilaka *et al.*, 2005), as shown in Fig. 5. The shape-index of the HS is a tool to visualize the presence of π–π stacking by the appearance of adjacent red and blue triangles. Fig. 5 clearly suggests that there are no significant π–π interactions in (I), as the above pattern is absent.

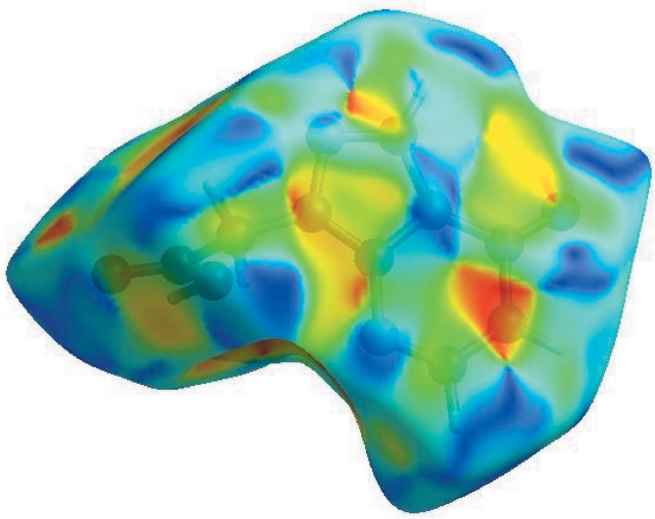

Figure 5
Hirshfeld surface of the title compound plotted over shape-index.

The overall two-dimensional fingerprint plot, Fig. 6*a*, and those delineated into H···O/O···H, H···N/N···H, H···H, H···C/C···H, C···O/O···C, N···O/O···N, C···N/N···C, C···C and O···O contacts (McKinnon *et al.*, 2007), and their relative contributions to the Hirshfeld surface, are illustrated in Fig. 6*b*–*j*. The most important interaction is H···O/O···H, contributing 34.8% to the overall crystal packing, which is shown in Fig. 6*b* where the pair of spikes have tips at $d_e + d_i$ = 1.81 Å. The pair of spikes in the fingerprint plot delineated into H···N/N···H contacts, Fig. 6*c*, with a 19.3% contribution to the HS has a symmetric distribution of points with the tips at $d_e + d_i$ = 1.74 Å. The H···H contacts contribute with 18.1% to the HS and are shown in Fig. 6*c* as widely scattered points of

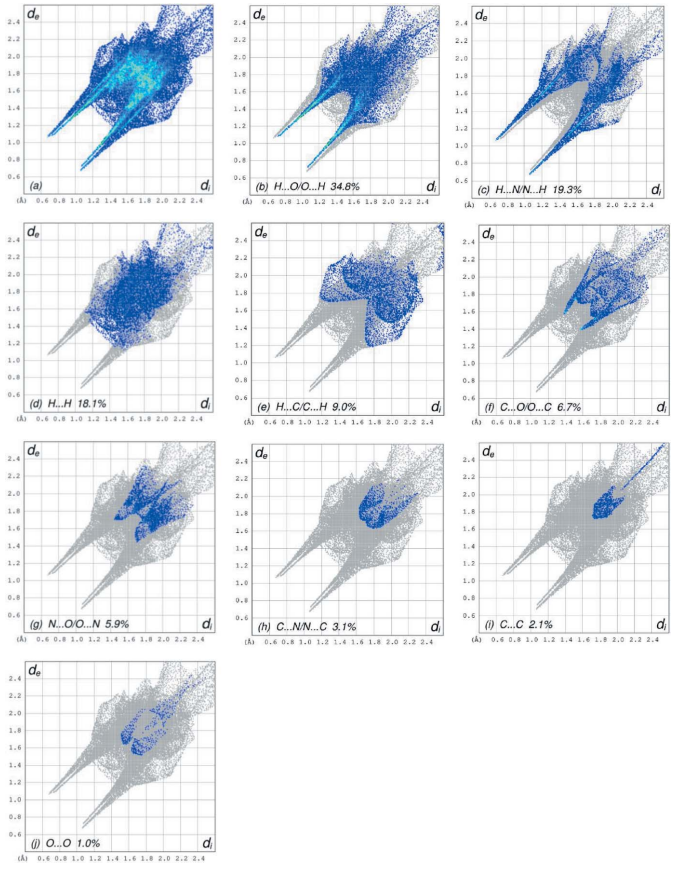

Figure 6
The full two-dimensional fingerprint plots for the title compound, showing (*a*) all interactions, and delineated into (*b*) H···O/O···H, (*c*) H···N/N···H, (*d*) H···H, (*e*) H···C/C···H, (*f*) C···O/O···C, (*g*) N···O/O···N, (*h*) C···N/N···C, (i) C···C and (*j*) O···O interactions. The d_i and d_e values are the closest internal and external distances (in Å) from given points on the Hirshfeld surface contacts.

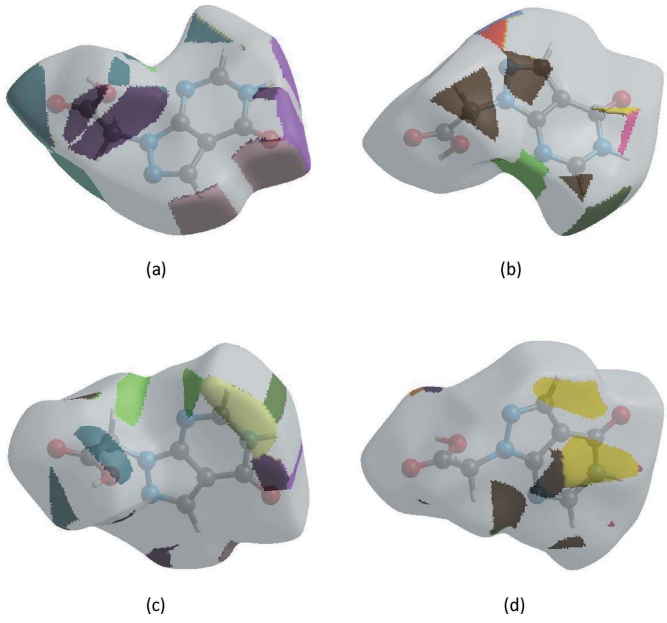

Figure 7
The Hirshfeld surface representations with the function d_{norm} plotted onto the surface for (*a*) H···O/O···H, (*b*) H···N/N···H, (*c*) H···H and (*d*) H···C/C···H interactions.

high density due to the large hydrogen content of the molecule with the tip at $d_e = d_i = 1.28$ Å. The high contribution of these interactions suggest that van der Waals interactions play the major role in the crystal packing (Hathwar *et al.*, 2015). The presence of C—H···π interactions is shown by the pair of wings in the fingerprint plot delineated into H···C/C···H contacts with the tips at $d_e + d_i = 2.93$ Å (Fig. 6*e*) with a 9.0% contribution to the HS. The C···O/O···C (Fig. 6*f*), N···O/O···N (Fig. 6*g*) and C···N/N···C (Fig. 6*h*) contacts contribute with 6.7%, 5.9% and 3.1%, respectively, to the HS and the distributions of points appear with the tips at $d_e + d_i = 2.95$ Å, $d_e + d_i = 3.15$ Å and $d_e + d_i = 3.38$ Å. The C···C contacts, Fig. 6*i*, with a 2.1% contribution to the HS, have a bullet-shaped distribution of points with the tip at $d_e = d_i = 1.73$ Å. Finally, the contribution of the O···O contacts (Fig. 6*j*) to the HS is 1.0% with a low density of points.

The Hirshfeld surface representations with the function d_{norm} plotted onto the surface are shown for the H···O/O···H, H···N/N···H, H···H and H···C/C···H interactions in Fig. 7*a*–*d*, respectively.

The strength of the crystal packing is important for determining the response to an applied mechanical force. If the crystal packing results in significant voids, then the molecules are not tightly packed and a small amount of applied external mechanical force may easily break the crystal. To check the mechanical stability of the crystal, a void analysis was performed by adding up the electron densities of the spherically symmetric atoms contained in the asymmetric unit (Turner *et al.*, 2011). The void surface is defined as an isosurface of the procrystal electron density and is calculated for the whole unit cell where the void surface meets the boundary of the unit cell and capping faces are generated to create an enclosed volume. The volume of the crystal voids (Fig. 8*a* and *b*) and the percentage of free space in the unit cell are calculated as 176.30 Å^3 and 10.94%, respectively. Thus, the crystal packing appears compact and the mechanical stability should be substantial.

5. Interaction energy and energy framework calculations

The intermolecular interaction energies were calculated using a CE–B3LYP/6–31G(d,p) energy model available in *Crystal Explorer* (Spackman *et al.*, 2021), where a cluster of molecules is generated by applying crystallographic symmetry operations with respect to a selected central molecule within the radius of 3.8 Å (Turner *et al.*, 2014). The total intermolecular energy (E_{tot}) is the sum of electrostatic (E_{ele}), polarization (E_{pol}), dispersion (E_{dis}) and exchange–repulsion (E_{rep}) energies (Turner *et al.*, 2015) with scale factors of 1.057, 0.740, 0.871 and 0.618, respectively (Mackenzie *et al.*, 2017). Hydrogen-bonding interaction energies (in kJ mol^{-1}) were calculated to be −73.0 (E_{ele}), −16.4 (E_{pol}), −27.3 (E_{dis}), 93.6 (E_{rep}) and −55.2 (E_{tot}) for N1—H1···O1 hydrogen-bonding interactions, −103.5 (E_{ele}), −22.1 (E_{pol}), −13.2 (E_{dis}), 98.8 (E_{rep}) and −76.3 (E_{tot}) for O2—H2*A*···N2 hydrogen-bonding interactions, −12.2 (E_{ele}), −2.9 (E_{pol}), −34.4 (E_{dis}), 19.9 (E_{rep}) and −32.8

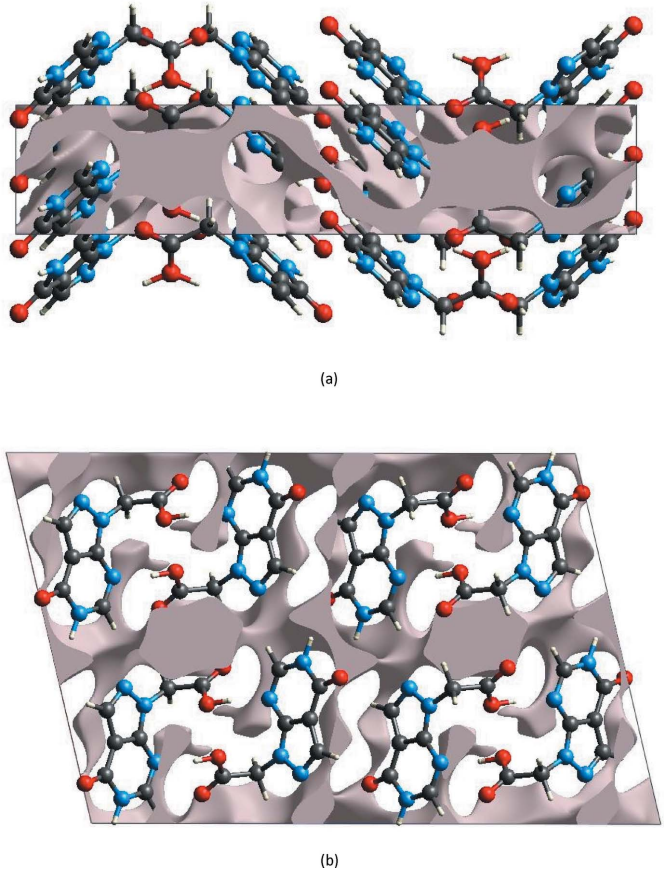

Figure 8
Graphical views of voids in the crystal packing of (I) (*a*) along the *a*-axis direction and (*b*) along the *b*-axis direction.

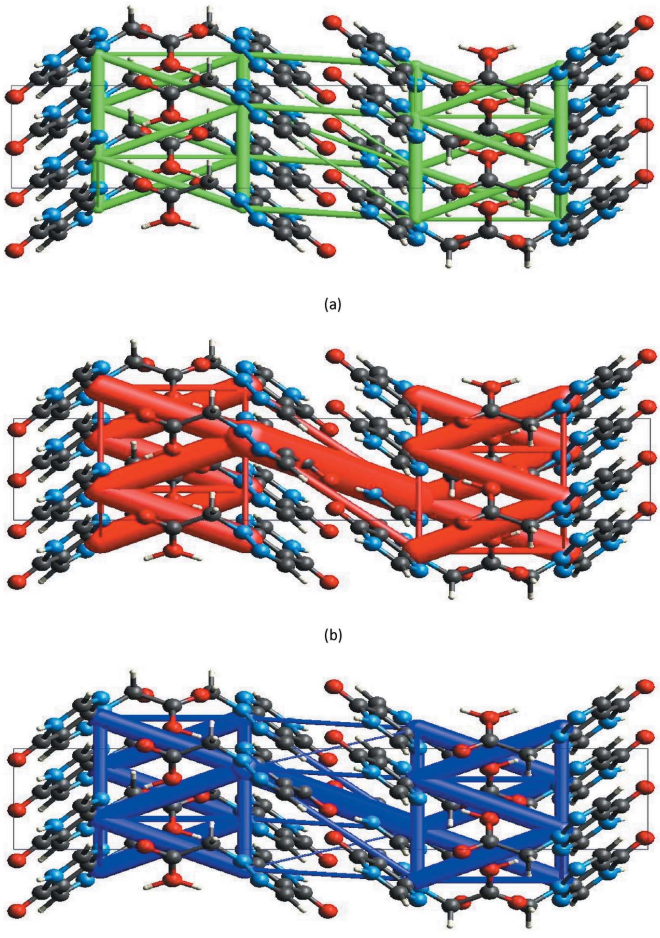

Figure 9
The energy framework for a cluster of molecules of (I) viewed down the *a*-axis direction (the *b* axis is vertical and the *c* axis is horizontal) showing (*a*) electrostatic energy, (*b*) dispersion energy and (*c*) total energy diagrams. The cylindrical radius is proportional to the relative strength of the corresponding energies and they were adjusted to the same scale factor of 80 with cut-off value of 5 kJ mol^{-1} within 1 × 1 × 1 unit cells.

(E_{tot}) for C5—H5···O1 hydrogen-bonding interactions, and −19.5 (E_{ele}), −3.2 (E_{pol}), −12.3 (E_{dis}), 23.8 (E_{rep}) and −19.0 (E_{tot}) for C6—H6*A*···O3 hydrogen-bonding interactions.

Energy frameworks combine the calculation of intermolecular interaction energies with a graphical representation of their magnitude (Turner *et al.*, 2015). Energies between molecular pairs are represented as cylinders joining the centroids of pairs of molecules with the cylinder radius proportional to the relative strength of the corresponding interaction energy. Energy frameworks were constructed for E_{ele} (red cylinders), E_{dis} (green cylinders) and E_{tot} (blue cylinders) (Fig. 9*a*, *b* and *c*). The results indicate that the stabilization is dominated *via* dispersion energy contributions in (I).

6. DFT and Molecular electrostatic potential (MEP) calculations

Density functional theory (DFT) using the standard B3LYP functional (Becke, 1993) and Pople's basis set 6–31G(d,p) implemented in *GAUSSIAN 09* (Frisch *et al.*, 2009) was used to optimize the molecular structure of (I) in the gas phase. The minimum was confirmed by frequency calculations, and the resulting optimized parameters (bond lengths and angles) agreed satisfactorily with the experimental structural data (Table 2). As a result, energies and other physico-chemical properties obtained from the optimized structure could be safely used to describe those of (I). The corresponding HOMO and LUMO energies were then used to estimate some parameters of global chemical reactivity, such as electronegativity (χ), hardness (η), ionization potential (I), electrophilicity (ω) and softness (σ) (Table 3). In addition, the molecular electrostatic potential (MEP) map, and dipole moment (μ) of (I) were similarly calculated.

Minor differences between theory and experiment are likely due to optimized values being obtained in the isolated gas phase, neglecting interactions in the solid phase. Briefly, the average O2—C7 and N4—C5 bond lengths calculated at

Table 2
Comparison of selected (X-ray and DFT) bond lengths and angles (Å, °).

	X-ray	B3LYP/6–311G(d,p)
O1═C1	1.2315 (17)	1.2450
O2—C7	1.3148 (17)	1.3767
O3═C7	1.2028 (17)	1.2273
N1—C2	1.3512 (18)	1.3749
N1—C1	1.3961 (18)	1.4047
N1—H1	0.9098	1.0128
N2═C2	1.3030 (18)	1.3131
N2—C3	1.3655 (17)	1.3742
N3—C3	1.3449 (17)	1.3605
N3—N4	1.3723 (16)	1.3955
N3—C6	1.4468 (17)	1.4417
C3═C4	1.3872 (19)	1.4048
N4═C5	1.3182 (19)	1.3412
C2—N1—C1	124.73 (11)	125.36
C2—N1—H1	121.4	120.93
C1—N1—H1	113.9	114.80
C2═N2—C3	112.91 (12)	113.46
C3—N3—N4	111.03 (11)	111.21
C3—N3—C6	128.49 (12)	128.12
N4—N3—C6	120.31 (11)	120.45
O1═C1—N1	120.51 (13)	120.02
O1═C1—C4	127.62 (13)	128.40
N2═C2—N1	124.94 (13)	124.12
O3═C7—O2	124.87 (13)	123.65
C2—N1—C1═O1	–176.82 (13)	–178.60
C3—N2—C2—N1	–0.6 (2)	–0.53
C1—N1—C2=N2	–1.4 (2)	–1.25
N4—N3—C3—N2	–178.88 (12)	–179.92

Table 3
Calculated energies.

Total energy, *TE* (eV)	–19449.75
E_{HOMO} (eV)	–6.66
E_{LUMO} (eV)	–1.41
Gap, ΔE (eV)	5.25
Dipole moment, μ (Debye)	4.49
Ionization potential, I (eV)	6.66
Electron affinity, A	1.42
Electronegativity, χ	4.04
Hardness, η	2.62
Electrophilicity index, ω	3.11
Softness, σ	0.38
Fraction of electron transferred, ΔN	0.56

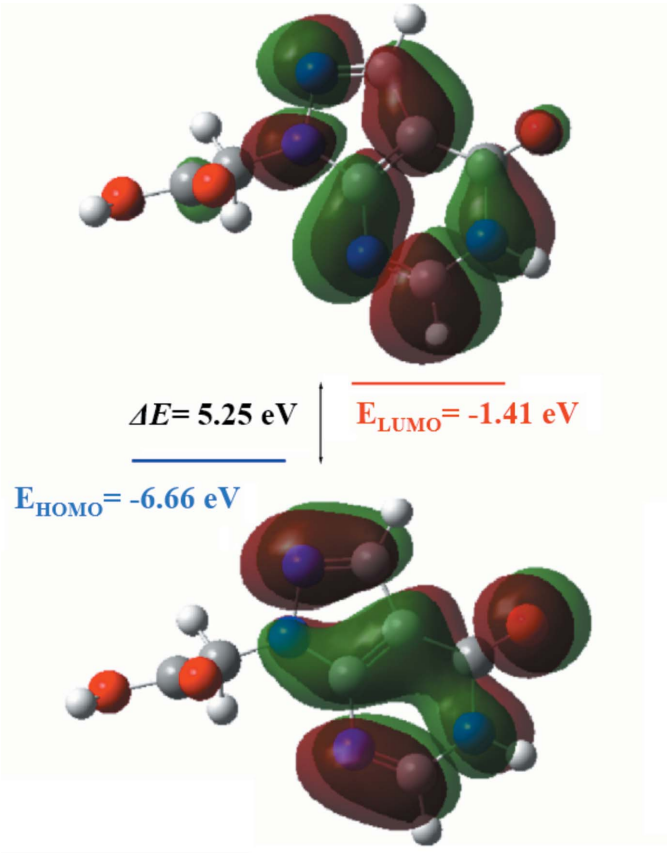

Figure 10
The optimized frontier molecular orbitals (HOMO and LUMO) with the energy band gap of (I).

the DFT/B3LYP/6-31G(d,p) level are 1.3767 and 1.3412 Å, respectively, which is slightly higher than the experimental values of 1.3148 (17) and 1.3182 (19) Å, respectively. Moreover, the torsion angles N4—N3—C3—N2 = −179.92° and C3—N2—C2—N1 = −0.53° agree well with the experimental ones of −178.88 (12) and −0.6 (2)°.

The optimized frontier molecular orbitals (HOMO and LUMO) are shown in Fig. 10. These orbitals play an important role in intramolecular charge transfer (ICT). The topological characteristics of these levels are important for interpreting kinetic stability and therefore potential chemical reactivity. The calculated energy band gap [$\Delta E = E_{LUMO} - E_{HOMO}$] of the molecule is 5.25 eV which indicates a hard molecule with low polarizability and low chemical and biological activities but high kinetic stability. The LUMO is mainly centered on the plane extending over the whole aromatic ring system of (I). The numerical reactivity descriptors, which are mainly based on HOMO–LUMO energies, are summarized in Table 3. The ionization potential (I) is defined as the amount of energy required to remove an electron from a molecule. The high ionization energy indicates also high stability and hence chemical inertness. Electron affinity (A) is defined as the energy released when an electron is added to a neutral molecule. Therefore a large value indicates the tendency of the molecule to retain its electrons. A negative chemical potential (μ) reflects molecular stability while hardness (η) characterizes the resistance of the cloud of molecular electrons to deformation during small disturbances. The overall electrophilicity index (ω) of a molecule is a measure of its stabilization energy following the addition of an external electronic charge or its resistance to exchange electron(s) with the system (Parr *et al.*, 1999). For (I), the ionization energy of 6.66 eV indicates high stability.

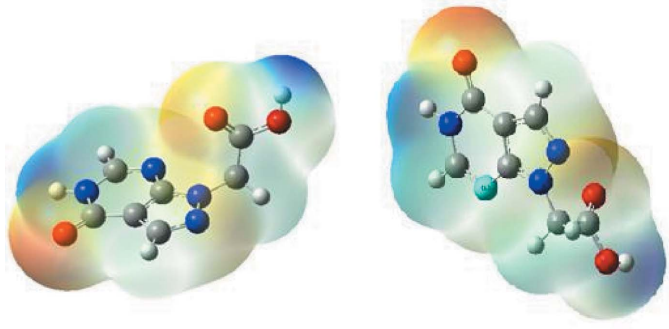

Figure 11
MEP surfaces of (I) mapped at the B3LYP/6–311G level.

The molecular electrostatic potential (MEP) of the surface was calculated on the optimized B3LYP/6-31G (d,p) level using *Gaussview* software (Frisch *et al.*, 2009). The MEP surface (Fig. 11) gives information about the reactive sites. The total electron density on which the electrostatic potential surface has been mapped is shown in Fig. 12 where a visual representation of chemically active sites and the comparative reactivity of atoms is also shown. The red regions denote the most negative electrostatic potential, the blue regions represent most positive electrostatic potential, and green regions represent the region of zero potential. Fig. 12 confirms the existence of intermolecular N—H···O, O—H···N and—H···O hydrogen-bonding interactions.

7. Database survey

A search of the Cambridge Structural Database (CSD, updated March 2022; Groom *et al.*, 2016) with the search fragment **A** (*R* = C—CH, C—C—OH; *R*′ = *R*" = variable;

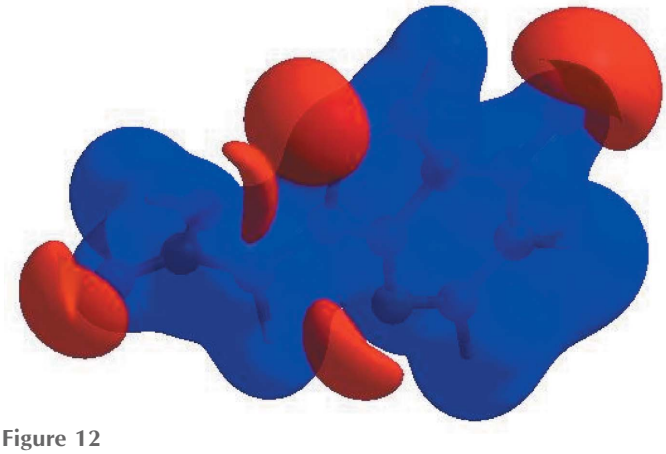

Figure 12
Contour surface of the electrostatic potential of (I).

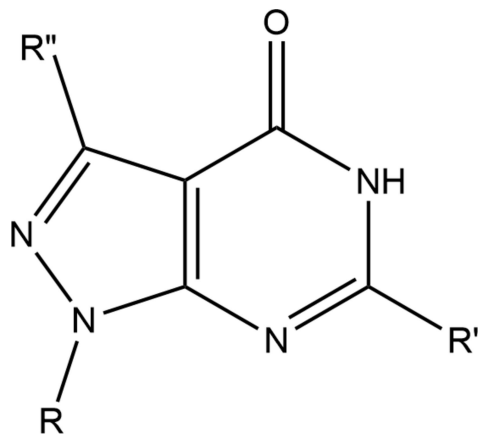

Figure 13
The molecular moiety used for the database search procedure.

Fig. 13) yielded 11 hits. These included structures with R = *t*-Bu, R" = H, R' = Ph (RULHEN; Liu *et al.*, 2015), *p*-anis (QIBVIH; Tan *et al.*, 2007); R" = H, R = *i*-Pr, R' = cyclobutanecarboxamido (QIBVON; Tan *et al.*, 2007), R = *n*-Bu, R' = benzamido (QIBWAA; Tan *et al.*, 2007), R = 3-phenylpropyl, R' = CH_3S (IFICUV; Avasthi *et al.*, 2002), R = 2-chloroethyl, R' = H (XAZRAT; Khazi *et al.*, 2012); R = 1-β-D-ribofuranosyl, R' = H, R" = OMe (FOVHIH; Anderson *et al.*, 1986), R' = NH_2, R" = H (YOMJIW; Ren *et al.*, 2019); R = 2-deoxy-β-D-*erythro*-pentofuranosyl, R' = NH_2, R" = Br (HIPPAX; Seela *et al.*, 1999), R" = I (HIPPEB; Seela *et al.*, 1999); R = 2-deoxy-2-fluoro-β-D-*arabino*-furanosyl, R' = NH_2, R" = Br (EJEJUY; He *et al.*, 2003). Like in (I), the pyrazolopyrimidine unit is essentially planar in these molecules, but with the variety of substituents and the presence of different hydrogen-bonding interactions, the packings in the crystal are quite different.

8. Refinement

Crystal data, data collection and structure refinement details are summarized in Table 4. Hydrogen atoms attached to carbon were placed in idealized positions while those attached to nitrogen and to oxygen were placed in locations derived from a difference-Fourier map and their parameters adjusted to give N—H = 0.91 and O—H = 0.87 Å. All H atoms were included as riding contributions with isotropic displacement parameters tied to those of the attached atoms.

9. Synthesis and crystallization

Ethyl 2-(4-oxo-4,5-dihydro-1*H*-pyrazolo[3,4-*d*]pyrimidin-1-yl)acetate (5 mmol) was dissolved in 10 ml of ethanol to which 10 ml of NaOH (aqueous, 10%$_{wt}$) were added. The reaction mixture was stirred magnetically at room temperature for 4 h. After evaporation of ethanol and washing the aqueous phase with ethyl acetate, the mixture was acidified with an aqueous solution of HCl (3 *N*). The formed precipitate was filtered off and rinsed with ether. The crude product was recrystallized from ethanol to obtain colourless crystals of (I) in 72% yield.

Table 4
Experimental details.

Crystal data	
Chemical formula	$C_7H_6N_4O_3$
M_r	194.16
Crystal system, space group	Monoclinic, *C*2/*c*
Temperature (K)	296
a, *b*, *c* (Å)	15.3747 (4), 4.6699 (1), 23.0423 (5)
β (°)	103.122 (1)
V (Å^3)	1611.20 (6)
Z	8
Radiation type	Cu $K\alpha$
μ (mm^{-1})	1.11
Crystal size (mm)	0.24 × 0.18 × 0.11
Data collection	
Diffractometer	Bruker D8 VENTURE PHOTON 100 CMOS
Absorption correction	Multi-scan (*SADABS*; Krause *et al.*, 2015)
T_{min}, T_{max}	0.81, 0.89
No. of measured, independent and observed [$I > 2\sigma(I)$] reflections	5850, 1598, 1503
R_{int}	0.026
(sin $\theta/\lambda)_{max}$ (Å^{-1})	0.625
Refinement	
$R[F^2 > 2\sigma(F^2)]$, $wR(F^2)$, S	0.048, 0.114, 1.16
No. of reflections	1598
No. of parameters	128
H-atom treatment	H-atom parameters constrained
$\Delta\rho_{max}$, $\Delta\rho_{min}$ (e Å^{-3})	0.25, −0.33

Computer programs: *APEX3* and *SAINT* (Bruker, 2016), *SHELXT* (Sheldrick, 2015*a*), *SHELXL* (Sheldrick, 2015*b*), *DIAMOND* (Brandenburg & Putz, 2012) and *publCIF* (Westrip, 2010).

Funding information

JTM acknowledges NSF–MRI grant No. 1228232 for the purchase of the diffractometer and Tulane University for support of the Tulane Crystallography Laboratory. TH is grateful to Hacettepe University Scientific Research Project Unit (grant No. 013 D04 602 004).

References

Anderson, J. D., Dalley, N. K., Revankar, G. R. & Robins, R. K. (1986). *J. Heterocycl. Chem.* **23**, 1869–1878.
Avasthi, K., Rawat, D. S., Sarkhel, S. & Maulik, P. R. (2002). *Acta Cryst.* C**58**, o325–o327.
Bakavoli, M., Bagherzadeh, G., Vaseghifar, M., Shiri, A., Pordel, M., Mashreghi, M., Pordeli, P. & Araghi, M. (2010). *Eur. J. Med. Chem.* **45**, 647–650.
Becke, A. D. (1993). *J. Chem. Phys.* **98**, 5648–5652.
Brandenburg, K. & Putz, H. (2012). *DIAMOND*. Crystal Impact GbR, Bonn, Germany.
Bruker (2016). *APEX3* and *SAINT*. Bruker AXS, Inc., Madison, Wisconsin, USA.
Dinakaran, V. S., Bomma, B. & Srinivasan, K. K. (2012). *Pharma Chem.* **4**, 255–265.
El Ghayati, L., Sert, Y., Sebbar, N. K., Ramli, Y., Ahabchane, N. H., Talbaoui, A., Mague, J. T., El Ibrahimi, B., Taha, M. L., Essassi, E. M., Al–Zaqri, N. & Alsalme, A. (2021). *J. Heterocycl. Chem.* **58**, 270–289.
El-Mekabaty, A. (2015). *Chem. Heterocycl. Compd*, **50**, 1698–1706.
El-Tombary, A. A. (2013). *Sci. Pharm.* **81**, 393–422.
Frisch, M. J., Trucks, G. W., Schlegel, H. B., Scuseria, G. E., Robb, M. A., Cheeseman, J. R., Scalmani, G., Barone, V., Mennucci, B., Petersson, G. A., Nakatsuji, H., Caricato, M., Li, X., Hratchian,

H. P., Izmaylov, A. F., Bloino, J., Zheng, G., Sonnenberg, J. L., Hada, M., Ehara, M., Toyota, K., Fukuda, R., Hasegawa, J., Ishida, M., Nakajima, T., Honda, Y., Kitao, O., Nakai, H., Vreven, T., Montgomery, J. A. Jr, Peralta, J. E., Ogliaro, F., Bearpark, M., Heyd, J. J., Brothers, E., Kudin, K. N., Staroverov, V. N., Kobayashi, R., Normand, J., Raghavachari, K., Rendell, A., Burant, J. C., Iyengar, S. S., Tomasi, J., Cossi, M., Rega, N., Millam, J. M., Klene, M., Knox, J. E., Cross, J. B., Bakken, V., Adamo, C., Jaramillo, J., Gomperts, R., Stratmann, R. E., Yazyev, O., Austin, A. J., Cammi, R., Pomelli, C., Ochterski, J. W., Martin, R. L., Morokuma, K., Zakrzewski, V. G., Voth, G. A., Salvador, P., Dannenberg, J. J., Dapprich, S., Daniels, A. D., Farkas, O., Foresman, J. B., Ortiz, J. V., Cioslowski, J. & Fox, D. J. (2009). *GAUSSIAN09*. Gaussian Inc., Wallingford, CT, USA.

Groom, C. R., Bruno, I. J., Lightfoot, M. P. & Ward, S. C. (2016). *Acta Cryst.* B**72**, 171–179.

Gudmundsson, K. S., Johns, B. A. & Weatherhead, J. (2009). *Bioorg. Med. Chem. Lett.* **19**, 5689–5692.

Gupta, S., Rodrigues, L. M., Esteves, A. P., Oliveira-Campos, A. M., Nascimento, M. S. J., Nazareth, N., Cidade, H., Neves, M. P., Fernandes, E., Pinto, M., Cerqueira, N. M. & Brás, N. (2008). *Eur. J. Med. Chem.* **43**, 771–780.

Hathwar, V. R., Sist, M., Jørgensen, M. R. V., Mamakhel, A. H., Wang, X., Hoffmann, C. M., Sugimoto, K., Overgaard, J. & Iversen, B. B. (2015). *IUCrJ*, **2**, 563–574.

He, J., Eickmeier, H. & Seela, F. (2003). *Acta Cryst.* C**59**, o406–o408.

Hirshfeld, H. L. (1977). *Theor. Chim. Acta*, **44**, 129–138.

Hni, B., Sebbar, N. K., Hökelek, T., El Ghayati, L., Bouzian, Y., Mague, J. T. & Essassi, E. M. (2019). *Acta Cryst.* E**75**, 593–599.

Holla, B. S., Mahalinga, M., Karthikeyan, M. S., Akberali, P. M. & Shetty, N. S. (2006). *Bioorg. Med. Chem.* **14**, 2040–2047.

Jayatilaka, D., Grimwood, D. J., Lee, A., Lemay, A., Russel, A. J., Taylor, C., Wolff, S. K., Cassam-Chenai, P. & Whitton, A. (2005). *TONTO -- A System for Computational Chemistry.* Available at: http://hirshfeldsurface.net/

Kandeel, M. M., Mohamed, L. W., Abd El Hamid, M. K. & Negmeldin, A. T. (2012). *Sci. Pharm.* **80**, 531–545.

Khazi, M. I. A., Fathima, N., Belavagi, N. S., Begum, N. S. & Khazi, I. M. (2012). *Acta Cryst.* E**68**, o2083.

Krause, L., Herbst-Irmer, R., Sheldrick, G. M. & Stalke, D. (2015). *J. Appl. Cryst.* **48**, 3–10.

Lahmidi, S., Sebbar, N. K., Hökelek, T., Chkirate, K., Mague, J. T. & Essassi, E. M. (2018). *Acta Cryst.* E**74**, 1833–1837.

Liu, M.-X., Li, J. R., Zheng, K., Yao, H., Zhang, Q. & Shi, D.-X. (2015). *Tetrahedron*, **71**, 7658–7662.

Mackenzie, C. F., Spackman, P. R., Jayatilaka, D. & Spackman, M. A. (2017). *IUCrJ*, **4**, 575–587.

Maher, M., Kassab, A. E., Zaher, A. F. & Mahmoud, Z. (2019). *J. Enzyme Inhib. Med. Chem.* **34**, 532–546.

McKinnon, J. J., Jayatilaka, D. & Spackman, M. A. (2007). *Chem. Commun.* pp. 3814–3816.

Parr, R. J., Szentpály, L., v, & Liu, S. (1999). *J. Am. Chem. Soc.* **121**, 1922–1924.

Ren, H., An, H. & Tao, J. (2019). *Molecules*, **24**, 983.

Sebbar, N. K., Mekhzoum, M. E. M., Essassi, E. M., Zerzouf, A., Talbaoui, A., Bakri, Y., Saadi, M. & Ammari, L. E. (2016). *Res. Chem. Intermed.* **42**, 6845–6862.

Seela, F., Becher, G., Rosemeyer, H., Reuter, H., Kastner, G. & Mikhailopulo, I. A. (1999). *Helv. Chim. Acta*, **82**, 105–124.

Severina, A. I., Georgiyants, V. A., Shtrygol, S. Yu. & Kavraiskyi, D. P. (2016). *Scr. Sci. Pharm.* **3**, 7–11.

Sheldrick, G. M. (2015*a*). *Acta Cryst.* A**71**, 3–8.

Sheldrick, G. M. (2015*b*). *Acta Cryst.* C**71**, 3–8.

Song, X. J., Shao, Y. & Dong, X. G. (2011). *Chin. Chem. Lett.* **22**, 1036–1038.

Spackman, M. A., McKinnon, J. J. & Jayatilaka, D. (2008). *CrystEngComm*, **10**, 377–388.

Spackman, P. R., Turner, M. J., McKinnon, J. J., Wolff, S. K., Grimwood, D. J., Jayatilaka, D. & Spackman, M. A. (2021). *J. Appl. Cryst.* **54**, 1006–1011.

Taia, A., Essaber, M., Aatif, A., Chkirate, K., Hökelek, T., Mague, J. T. & Sebbar, N. K. (2020). *Acta Cryst.* E**76**, 962–966.

Tan, T. M. C., Yang, F., Fu, H., Raghavendra, M. S. & Lam, Y. (2007). *J. Comb. Chem.* **9**, 210–218.

Turner, M. J., Grabowsky, S., Jayatilaka, D. & Spackman, M. A. (2014). *J. Phys. Chem. Lett.* **5**, 4249–4255.

Turner, M. J., McKinnon, J. J., Jayatilaka, D. & Spackman, M. A. (2011). *CrystEngComm*, **13**, 1804–1813.

Turner, M. J., Thomas, S. P., Shi, M. W., Jayatilaka, D. & Spackman, M. A. (2015). *Chem. Commun.* **51**, 3735–3738.

Venkatesan, P., Thamotharan, S., Ilangovan, A., Liang, H. & Sundius, T. (2016). *Spectrochim. Acta Part A*, **153**, 625–636.

Westrip, S. P. (2010). *J. Appl. Cryst.* **43**, 920–925.

Zhang, C., Zhou, Q., Wu, X. N., Huang, Y. D., Zhou, J., Lai, Z., Wu, Y. & Luo, H. B. (2018). *J. Enzyme Inhib. Med. Chem.* **33**, 260–270.

supporting information

Acta Cryst. (2022). E**78**, 953-960 [https://doi.org/10.1107/S2056989022008489]

Crystal structure determination, Hirshfeld surface, crystal void, intermolecular interaction energy analyses, as well as DFT and energy framework calculations of 2-(4-oxo-4,5-dihydro-1*H*-pyrazolo[3,4-*d*]pyrimidin-1-yl)acetic acid

Ezaddine Irrou, Younesse Ait Elmachkouri, Ali Oubella, Hassan Ouchtak, Samira Dalbouha, Joel T. Mague, Tuncer Hökelek, Lhoussaine El Ghayati, Nada Kheira Sebbar and Mohamed Labd Taha

Computing details

Data collection: *APEX3* (Bruker, 2016); cell refinement: *SAINT* (Bruker, 2016); data reduction: *SAINT* (Bruker, 2016); program(s) used to solve structure: *SHELXT* (Sheldrick, 2015*a*); program(s) used to refine structure: *SHELXL* (Sheldrick, 2015*b*); molecular graphics: *DIAMOND* (Brandenburg & Putz, 2012); software used to prepare material for publication: *publCIF* (Westrip, 2010).

2-(4-Oxo-4,5-dihydro-1*H*-pyrazolo[3,4-*d*]pyrimidin-1-yl)acetic acid

Crystal data

$C_7H_6N_4O_3$
M_r = 194.16
Monoclinic, *C*2/*c*
a = 15.3747 (4) Å
b = 4.6699 (1) Å
c = 23.0423 (5) Å
β = 103.122 (1)°
V = 1611.20 (6) Å^3
Z = 8
F(000) = 800
D_x = 1.601 Mg m^{-3}
Cu *Kα* radiation, *λ* = 1.54178 Å
Cell parameters from 5261 reflections
θ = 3.9–74.4°
μ = 1.11 mm^{-1}
T = 296 K
Block, colourless
0.24 × 0.18 × 0.11 mm

Data collection

Bruker D8 VENTURE PHOTON 100 CMOS diffractometer
Radiation source: INCOATEC I*μ*S micro–focus source
Mirror monochromator
Detector resolution: 10.4167 pixels mm^{-1}
ω scans
Absorption correction: multi-scan (*SADABS*; Krause *et al.*, 2015)
T_{min} = 0.81, T_{max} = 0.89
5850 measured reflections
1598 independent reflections
1503 reflections with $I > 2\sigma(I)$
R_{int} = 0.026
θ_{max} = 74.4°, θ_{min} = 3.9°
h = −16→18
k = −5→5
l = −28→28

Refinement

Refinement on F^2
Least-squares matrix: full
$R[F^2 > 2\sigma(F^2)]$ = 0.048
$wR(F^2)$ = 0.114
S = 1.16
1598 reflections

128 parameters
0 restraints
Primary atom site location: dual
Secondary atom site location: difference Fourier map
Hydrogen site location: mixed
H-atom parameters constrained

$w = 1/[\sigma^2(F_o^2) + (0.063P)^2 + 0.6265P]$ where $P = (F_o^2 + 2F_c^2)/3$
$(\Delta/\sigma)_{max} < 0.001$
$\Delta\rho_{max} = 0.25$ e Å^{-3}
$\Delta\rho_{min} = -0.33$ e Å^{-3}
Extinction correction: *SHELXL 2018/3* (Sheldrick, 2015*b*), $Fc^*=kFc[1+0.001xFc^2\lambda^3/\sin(2\theta)]^{-1/4}$
Extinction coefficient: 0.0304 (14)

Special details

Geometry. All esds (except the esd in the dihedral angle between two l.s. planes) are estimated using the full covariance matrix. The cell esds are taken into account individually in the estimation of esds in distances, angles and torsion angles; correlations between esds in cell parameters are only used when they are defined by crystal symmetry. An approximate (isotropic) treatment of cell esds is used for estimating esds involving l.s. planes.

Refinement. Refinement of F^2 against ALL reflections. The weighted R-factor wR and goodness of fit S are based on F^2, conventional R-factors R are based on F, with F set to zero for negative F^2. The threshold expression of $F^2 > 2\text{sigma}(F^2)$ is used only for calculating R-factors(gt) etc. and is not relevant to the choice of reflections for refinement. R-factors based on F^2 are statistically about twice as large as those based on F, and R- factors based on ALL data will be even larger. H-atoms attached to carbon were placed in calculated positions (C—H = 0.95 - 0.99 Å) while those attached to nitrogen and to oxygen were placed in locations derived from a difference map and their parameters adjusted to give N—H = 0.91 and O—H = 0.87 Å. All were included as riding contributions with isotropic displacement parameters 1.2 - 1.5 times those of the attached atoms.

Fractional atomic coordinates and isotropic or equivalent isotropic displacement parameters (Å^2)

	x	*y*	*z*	U_{iso}*/U_{eq}
O1	0.39351 (7)	0.6126 (2)	0.49522 (5)	0.0517 (4)
H1	0.491406	0.298878	0.457379	0.078*
O2	0.17845 (7)	0.3011 (2)	0.24916 (4)	0.0474 (3)
H2A	0.169736	0.370596	0.213269	0.071*
O3	0.07906 (7)	−0.0274 (3)	0.20612 (5)	0.0586 (4)
N1	0.43440 (7)	0.2658 (3)	0.43684 (5)	0.0417 (3)
N2	0.33583 (7)	0.0013 (3)	0.36309 (5)	0.0397 (3)
N3	0.18190 (7)	0.1198 (3)	0.35967 (5)	0.0375 (3)
C1	0.37053 (9)	0.4290 (3)	0.45639 (6)	0.0389 (4)
C2	0.41582 (9)	0.0694 (3)	0.39270 (6)	0.0421 (4)
H2	0.463751	−0.024383	0.382697	0.051*
C3	0.27031 (9)	0.1489 (3)	0.38153 (5)	0.0353 (3)
C4	0.28199 (9)	0.3561 (3)	0.42577 (5)	0.0376 (3)
N4	0.13470 (8)	0.3040 (3)	0.38734 (5)	0.0435 (3)
C5	0.19481 (10)	0.4438 (3)	0.42717 (6)	0.0438 (4)
H5	0.181431	0.582221	0.452827	0.053*
C6	0.13600 (9)	−0.0569 (3)	0.31065 (6)	0.0410 (4)
H6A	0.076673	−0.099206	0.316240	0.049*
H6B	0.167753	−0.237123	0.311870	0.049*
C7	0.12731 (8)	0.0757 (3)	0.24955 (6)	0.0387 (4)

Atomic displacement parameters (Å²)

	U^{11}	U^{22}	U^{33}	U^{12}	U^{13}	U^{23}
O1	0.0478 (6)	0.0593 (7)	0.0440 (6)	−0.0021 (5)	0.0021 (4)	−0.0198 (5)
O2	0.0562 (6)	0.0484 (6)	0.0337 (5)	−0.0094 (5)	0.0024 (4)	0.0066 (4)
O3	0.0537 (7)	0.0787 (8)	0.0370 (6)	−0.0145 (6)	−0.0030 (5)	−0.0075 (5)
N1	0.0377 (6)	0.0487 (7)	0.0362 (6)	−0.0022 (5)	0.0031 (5)	−0.0063 (5)
N2	0.0409 (6)	0.0435 (6)	0.0333 (6)	−0.0011 (5)	0.0057 (5)	−0.0058 (5)
N3	0.0373 (6)	0.0434 (6)	0.0300 (6)	−0.0026 (5)	0.0040 (4)	−0.0002 (4)
C1	0.0435 (7)	0.0425 (7)	0.0293 (6)	−0.0021 (6)	0.0050 (5)	−0.0036 (5)
C2	0.0418 (7)	0.0470 (8)	0.0366 (7)	0.0006 (6)	0.0069 (6)	−0.0051 (6)
C3	0.0380 (7)	0.0392 (7)	0.0278 (6)	−0.0021 (5)	0.0056 (5)	0.0016 (5)
C4	0.0405 (7)	0.0425 (7)	0.0290 (6)	−0.0013 (5)	0.0062 (5)	−0.0019 (5)
N4	0.0415 (6)	0.0525 (7)	0.0364 (6)	0.0021 (5)	0.0087 (5)	−0.0001 (5)
C5	0.0452 (8)	0.0510 (8)	0.0348 (7)	0.0026 (6)	0.0081 (6)	−0.0050 (6)
C6	0.0418 (7)	0.0433 (8)	0.0348 (7)	−0.0092 (6)	0.0018 (5)	−0.0003 (5)
C7	0.0354 (7)	0.0446 (8)	0.0336 (7)	0.0004 (5)	0.0024 (5)	−0.0018 (5)

Geometric parameters (Å, º)

O1—C1	1.2315 (17)	N3—C6	1.4468 (17)
O2—C7	1.3148 (17)	C1—C4	1.4251 (18)
O2—H2A	0.8701	C2—H2	0.9300
O3—C7	1.2028 (17)	C3—C4	1.3872 (19)
N1—C2	1.3512 (18)	C4—C5	1.4090 (19)
N1—C1	1.3961 (18)	N4—C5	1.3182 (19)
N1—H1	0.9098	C5—H5	0.9300
N2—C2	1.3030 (18)	C6—C7	1.5160 (18)
N2—C3	1.3655 (17)	C6—H6A	0.9700
N3—C3	1.3449 (17)	C6—H6B	0.9700
N3—N4	1.3723 (16)		
C7—O2—H2A	110.0	C3—C4—C5	104.74 (12)
C2—N1—C1	124.73 (11)	C3—C4—C1	118.71 (12)
C2—N1—H1	121.4	C5—C4—C1	136.54 (13)
C1—N1—H1	113.9	C5—N4—N3	105.83 (11)
C2—N2—C3	112.91 (12)	N4—C5—C4	111.12 (13)
C3—N3—N4	111.03 (11)	N4—C5—H5	124.4
C3—N3—C6	128.49 (12)	C4—C5—H5	124.4
N4—N3—C6	120.31 (11)	N3—C6—C7	114.60 (11)
O1—C1—N1	120.51 (13)	N3—C6—H6A	108.6
O1—C1—C4	127.62 (13)	C7—C6—H6A	108.6
N1—C1—C4	111.86 (11)	N3—C6—H6B	108.6
N2—C2—N1	124.94 (13)	C7—C6—H6B	108.6
N2—C2—H2	117.5	H6A—C6—H6B	107.6
N1—C2—H2	117.5	O3—C7—O2	124.87 (13)
N3—C3—N2	125.93 (12)	O3—C7—C6	121.10 (13)
N3—C3—C4	107.27 (12)	O2—C7—C6	113.99 (11)

N2—C3—C4	126.80 (12)		
C2—N1—C1—O1	−176.82 (13)	O1—C1—C4—C3	177.49 (14)
C2—N1—C1—C4	2.4 (2)	N1—C1—C4—C3	−1.64 (18)
C3—N2—C2—N1	−0.6 (2)	O1—C1—C4—C5	−1.6 (3)
C1—N1—C2—N2	−1.4 (2)	N1—C1—C4—C5	179.24 (15)
N4—N3—C3—N2	−178.88 (12)	C3—N3—N4—C5	−0.97 (15)
C6—N3—C3—N2	−3.7 (2)	C6—N3—N4—C5	−176.57 (12)
N4—N3—C3—C4	0.92 (15)	N3—N4—C5—C4	0.64 (16)
C6—N3—C3—C4	176.06 (12)	C3—C4—C5—N4	−0.10 (16)
C2—N2—C3—N3	−179.00 (13)	C1—C4—C5—N4	179.09 (15)
C2—N2—C3—C4	1.2 (2)	C3—N3—C6—C7	−83.22 (17)
N3—C3—C4—C5	−0.49 (15)	N4—N3—C6—C7	91.53 (15)
N2—C3—C4—C5	179.30 (13)	N3—C6—C7—O3	−168.31 (14)
N3—C3—C4—C1	−179.86 (11)	N3—C6—C7—O2	13.70 (18)
N2—C3—C4—C1	−0.1 (2)		

Hydrogen-bond geometry (Å, º)

*Cg*1 is the centroid of the C3/C4/C5/N4/N3 ring.

D—H···*A*	*D*—H	H···*A*	*D*···*A*	*D*—H···*A*
N1—H1···O1^{i}	0.91	1.90	2.8094 (16)	175
O2—H2*A*···N2^{ii}	0.87	1.85	2.7120 (14)	173
C5—H5···O1^{iii}	0.93	2.33	3.2305 (18)	164
C6—H6*A*···O3^{iv}	0.97	2.36	3.2436 (18)	152
C6—H6*B*···*Cg*1^{v}	0.97	2.98	3.7387 (15)	136

Symmetry codes: (i) −*x*+1, −*y*+1, −*z*+1; (ii) −*x*+1/2, *y*+1/2, −*z*+1/2; (iii) −*x*+1/2, −*y*+3/2, −*z*+1; (iv) −*x*, *y*, −*z*+1/2; (v) *x*, *y*−1, *z*.